Differential influence of anticancer treatments and angiogenesis on the seric titer of autoantibody used as tumor and metastasis biomarker

Defresne, Florence; Bouzin, Caroline; Guilbaud, Céline; Dieu, Marc; Delaive, Edouard; Michiels, Carine; Raes, Martine; Feron, Olivier

Published in:
Neoplasia

DOI:
10.1593/neo.10238

Publication date:
2010

Document Version
Publisher's PDF, also known as Version of record

NEOPLASIA
www.neoplasia.com

Volume 12 Number 7 July 2010 pp. 562–570 562

Differential Influence of Anticancer Treatments and Angiogenesis on the Seric Titer of Autoantibody Used as Tumor and Metastasis Biomarker[1,2]

Florence Defresne*, Caroline Bouzin*, Céline Guilbaud*, Marc Dieu†, Edouard Delaive†, Carine Michiels†, Martine Raes† and Olivier Feron*

*Angiogenesis and Cancer Research Laboratory, Pole of Pharmacology and Therapeutics, Université catholique de Louvain, Brussels, Belgium; †Laboratory of Biochemistry and Cellular Biology, University of Namur-FUNDP, Namur, Belgium

Abstract

Early detection of tumor-specific autoantibodies (auto-Abs) has the potential to be used for cancer screening and diagnosis. Whether auto-Ab may be useful to track metastatic progression or response to treatment is, however, largely unknown. To address these issues, the serological proteome was analyzed in an invasive but treatment-responsive mouse tumor model. Among 40 serum-reactive proteins identified by multiplex analysis, we chose to focus on glucose-regulated protein 78 (GRP78), a chaperone protein involved in the endoplasmic reticulum stress response. We first validated GRP78 as a protein overexpressed and mislocalized in tumor cells. We then documented that an increase in GRP78 auto-Ab titer preceded the detection of a palpable tumor mass, correlated with metastatic progression, and was influenced by the onset of tumor neovascularization. We also found that chemotherapy and radiotherapy, both leading to inhibition of tumor growth, oppositely influenced the anti-GRP78 immune response. Whereas radiation increased the concentration of GRP78 auto-Ab by three-fold, the auto-Ab titer was reduced in response to bolus or metronomic administration of cyclophosphamide. Finally, we established a decrease in auto-Ab–producing B lymphocytes in response to chemotherapy and the overexpression of GRP78 together with a strong immunoglobulin response in irradiated tumors. In conclusion, we identified GRP78 auto-Ab as an early marker of tumor and metastatic progressions. However, the multiple influences of anticancer treatments on the humoral immune system calls for caution when exploiting such auto-Ab as markers of the tumor response.

Neoplasia (2010) 12, 562–570

Introduction

Autoantibodies (auto-Ab) are present in the blood of patients who are affected by different malignancies [1,2]. These antibodies are directed against a group of autologous cellular antigens generally known as tumor-associated antigens (TAAs) [3–5]. The expression by tumor cells of proteins, which are mutated, mislocalized, or produced in abnormal quantities, is thought to mainly account for this humoral response. Auto-Abs circulate for a longer time than other polypeptides because they are very stable in the serum and often produced in large amounts. Their biochemical properties are well understood, and many available reagents do exist for their detection. Serum profiling of circulating auto-Ab is therefore considered a very attractive method to diagnose cancer at early stages.

Different proteomic techniques allow detecting auto-Ab and identifying TAAs: serological expression cloning and serological proteome analysis (SERPA) are among them [6–9]. These methods use a patient's sera to probe blotted phage expression libraries derived from tumor cells or tumor cell lysates blotted onto a membrane after two-dimensional gel separation, respectively. Modification of the latter involves spotting

Abbreviations: auto-Ab, autoantibody; SERPA, serological proteome analysis; TAA, tumor-associated antigen

Address all correspondence to: Prof. Olivier Feron, Pole of Pharmacology and Therapeutics, Université catholique de Louvain – FATH5349, 52 Ave E. Mounier, B-1200 Brussels, Belgium. E-mail: olivier.feron@uclouvain.be

[1]This work was supported by grants from the Fonds de la Recherche Scientifique Médicale, the Fonds National de la Recherche Scientifique (FNRS), the Télévie, the Belgian Federation Against Cancer, the J. Maisin Foundation, and the Région Bruxelles-Capitale and by an Action de Recherche Concertée (ARC 09/14-020) from the Communauté Française de Belgique. F.D. is FNRS Research Assistant and O.F. is FNRS Research Director.

[2]This article refers to supplementary materials, which are designated by Tables W1 and W2 and Figures W1 and W2 and are available online at www.neoplasia.com.

Received 3 February 2010; Revised 28 March 2010; Accepted 29 March 2010

DOI 10.1593/neo.10238

of fractionated tumor lysates onto microarrays [10], and for each of these techniques, final identification of the proteins of interest requires mass spectrometry. SERPA has the advantages to allow proteins with their posttranslational modifications to be analyzed for their immunogenicity and to reveal, in a single experiment, the global reactivity of a given serum toward a tumor-derived proteome. Multiple studies have already used these techniques to identify auto-Abs in a variety of cancers including hepatocellular carcinoma [3], colon cancer [11,12], lung cancer [13], and breast cancer [5,14].

Very little is known, however, about how the auto-Ab–based markers of early cancer stages do evolve when the disease progresses to metastases or when patients undergo anticancer treatments. In theory, the ideal auto-Ab candidate would have to be upregulated when the tumor is growing or when metastases are developing and to fall down when the patients respond to the treatment. Collateral effects of treatments on the capacity of tumor or immune cells to contribute to the auto-Ab response, however, should not be underestimated. Chemotherapy may, for instance, lead to lymphodepletion and thereby interfere with the capacity of the humoral immune system to produce auto-Ab. Whether a reduction in auto-Ab reflects the effects of chemotherapy on tumor growth or instead acknowledges a systemic interference with the immune system needs to be addressed to fully exploit information derived from serological proteome analyses.

Here, we applied the SERPA technique to identify the fate of auto-Ab in tumor-bearing mice exposed to different treatments, including chemotherapy, radiotherapy, and surgery. Such an animal model allows to reduce interindividual serological variations under basal conditions as well as in response to treatments and to concentrate in 2 to 3 weeks, the life of a tumor from the primary tumor emergence to the metastases development. Using SERPA technology, we identified glucose-regulated protein 78 (GRP78) as a reproducible immunogenic TAA in our mouse tumor model. A specific enzyme-linked immunosorbent assay (ELISA) was developed and confirmed that the increase in GRP78 auto-Ab titer was correlated with primary tumor and metastases development. Opposite variations in the GRP78 auto-Ab concentrations after chemotherapy and radiotherapy, however, pointed out how treatment-driven modulation of the immune system may interfere with the auto-Ab production and detection.

Materials and Methods

Cells and Mice

Lewis lung carcinoma (LLc) cells were routinely cultured in 175-mm flasks in serum containing Dulbecco modified Eagle medium (Invitrogen, Paisley, UK). Adult C57Bl/6J mice (Elevage Janvier, Le Genest Saint-Isle, France) received intramuscular injections of 10^6 syngeneic LLc cells in the posterior right leg. The tumor diameters were regularly tracked with an electronic caliper. Blood was collected for serological assays through retro-orbital or intracardiac routes according to the required amounts. Ten days after tumor cell injection, mice were exposed to radiotherapy or chemotherapy. Local irradiation was administered to mice using a RT-250 device (Philips Medical Systems, Brussels, Belgium) with a dose delivery of 1.2 Gy/min. The tumor was centered in a circular irradiation field, and healthy tissues were protected by a lead mask. Two different protocols were used for chemotherapy: cyclophosphamide (Bayer, Leverkusen, Germany) was either administered through intraperitoneal injection of a bolus dose (100 mg/kg) or added to the drinking water (renewed every 3 days) for a so-called metronomic administration [15] to reach a 20-mg/kg per day regimen. Each procedure was approved by local authorities according to national animal care regulations.

SERPA Technique

Tumors from three different mice were pooled, lysed in difference in-gel electrophoresis labeling buffer (7 M urea, 2 M thiourea, 4% 3-[(3-cholamidopropyl)dimethylammonio]-1-propanesulfonate, and 30 mM Tris pH 8.5), homogenized using Ultra-Turrax T25 (IKA, Staufen, Germany), and clarified by centrifuging at 12,000*g* for 15 minutes at 4°C. Protein concentration was determined by the Bradford method, and extracts were diluted to reach a final concentration of 5 to 10 μg/μl. pH was adjusted to 8.5, and 25 μg of each sample was labeled with 200 pmol of amine-reactive cyanine Cy5 dye (Amersham GE Healthcare, Diegem, Belgium) for 30 minutes in the dark at 4°C, according to the manufacturer's instructions. Labeling reaction was stopped by incubating the mixture for 10 minutes with 10 mM lysine (Sigma Aldrich, Bornem, Belgium), and nonlabeled proteins were added to reach 300 μg. Samples were then diluted in immobilized pH gradient (IPG) buffer (4% 3-[(3-cholamidopropyl)dimethylammonio]-1-propanesulfonate, 7 M urea, 2 M thiourea, 30 mM Tris, 30 mM DTT, 1% IPG buffer 3-11 (vol./vol.) [Amersham GE Healthcare]) and incubated for 20 minutes in the dark at room temperature.

Proteins were loaded onto rehydrated 18-cm IPGstrips pH 3-11 NL for the isoelecteric focusing on the IPGphor; parameters were as follows: 300 V for 3 hours, gradient steps of 1000 V for 8 hours, 8000 V for 3 hours, and 8000 V for 45 minutes at 20°C with a maximum current setting of 50 μA per strip. IPGstrips were subsequently incubated for 15 minutes with equilibration solutions (6 M urea, 30% glycerol, 2% SDS, 1.5 M Tris pH 8.8) supplemented with 10 mg/ml DTT and 25 mg/ml iodoacetamide, respectively. One-dimensional strips were then washed and loaded onto the two-dimensional gels (10% acrylamide). Electrophoresis was performed overnight at 15°C.

Separated proteins were finally transferred onto low-fluorescence polyvinylidene difluoride (PVDF) membrane (200 mA for 2 hours). All the materials and products were purchased from GE Healthcare, except glycerol which was purchased from Sigma. Blotted two-dimensional membranes were incubated for 3 hours in 5% nonfat dry milk containing Tris–Tween buffered saline (TTBS) blocking buffer and were then exposed overnight to either control mouse serum or tumor-bearing mice (dilution, 1:100); a pool of sera collected from 15 different mice was used per condition. After several washes in TTBS containing 1% nonfat dry milk, membranes were incubated with horseradish peroxidase–conjugated goat antimouse immunoglobulin class G (IgG) antibody (1:5000; Jackson Immunoresearch, Sulfolk, UK) for 2 hours. Note that this secondary antibody (cat. no. 115-035) reacts with both heavy and light chains of IgG molecules and may thus also react with other immunoglobulin classes, including IgM. Immunodetection was performed using ECL Plus (GE Healthcare) followed by scanning at the Cy2 wavelength on the Ettan Dige Imager (GE Healthcare; Figure W1).

Immunoblot Analysis and Immunocytochemistry

Collected tumors were homogenized with an Ultra-Turrax in RIPA lysis buffer containing 1% protease inhibitor cocktail. SDS-PAGE was performed as previously described on 10% acrylamide gels, and after transfer, PVDF membranes were probed overnight at 4°C with anti-GRP78 antibodies (BD Pharmingen [Erembodegem, Belgium] and Cell Signaling [Danvers, MA]). HRP-conjugated secondary antibody was used for detection with ECL Plus.

For immunohistochemical analyses, frozen tumor sections were probed overnight at 4°C with anti-GRP78 antibody (dilution 1:50; Cell Signaling) or with anti-CD31 antibody (dilution, 1:50; Pharmingen) after a 30-minute blocking procedure in PBS containing 0.1% Tween and 5% BSA. Detection was performed with Alexa Fluor secondary antibodies (dilution, 1:300); quantification was performed using ImageJ software (National Institutes of Health, Bethesda, MD). In some experiments, nonpermeabilized tumor sections were costained with rhodamine-labeled wheat germ agglutinin (Vector Laboratories, Burlingame, CA) to probe plasma membranes.

Laser Doppler Imaging

Local tumor blood flow was measured with a laser Doppler imager (Moor Instruments, Devon, UK). Mice were anesthetized, and fur was removed using a depilatory cream. The animals were placed on a heating pad (37°C) to minimize variations in temperature. The perfusion of the tumor-bearing and control legs can be evaluated on the basis of colored histogram pixels.

In-gel Enzymatic Digestion and Mass Spectrometry

Preparative gels were performed with 300 μg of unlabeled proteins according to the protocol described above for the analytical gels. Two-dimensional gels were krypton-stained (Pierce, Rockford, IL) after protein fixation. The proteins of interest were automatically picked from the gels with the Ettan Spot Picker (GE Healthcare). After rinsing, gel pieces were dehydrated in acetonitrile and further dried at 37°C for 20 minutes. Digestion was performed overnight with trypsin (12.5 ng/μl) in 50 mM ammonium bicarbonate. The extraction step was performed with formic acid 5% for 15 minutes at 37°C. Peptides were extracted with 5% formic acid at 37°C for 15 minutes, and the collected supernatants were kept frozen at −20°C until mass spectrometry analysis.

Digested peptides were then processed for identification on the basis of their mass fingerprint obtained using a matrix-assisted laser desorption/ionization–time of flight mass spectrometry (MALDI-TOF; Waters, Milford, MA) or using a nanoflow liquid chromatography coupled to tandem mass spectrometry with electrospray ionization (Waters) on a CapLC Q-TOF2 mass spectrometer (Waters; Supplementary Data for detailed information). Full-length proteins were identified with Mascot software (version 2.2; Matrix Sciences, London, UK) by sequence homology research against mouse protein databases.

GRP78 ELISA

Amounts of circulating auto-Abs to GRP78 were determined by conventional ELISA. Ninety-six–well plates (Reacti-Bind; Thermo Scientific, Rockford, IL) were coated overnight at room temperature with 5 μg/ml recombinant GRP78 protein (Stressgen, Ann Arbor, MI). Coating and blocking procedures were carried out using Ultrablock and Neptune buffers from AbD Serotec (Oxford, UK) according to the manufacturer's instructions. Sera (dilution, 1:100) were incubated overnight at 4°C, and after washing, specific hybridization was measured with a peroxidase-conjugated antimouse IgG antibody (dilution, 1:10,000) and addition of 3,3′,5,5′-tetramethylbenzidine (Merck Chemicals, Nottingham, UK). Plates were read at 450 nm in a microplate reader (VictorX4; Perkin Elmer, Waltham, MA), and the calibration curve was performed for each single experiment using serial dilutions of GRP78 antibody (BD Pharmingen; Figure W2).

Immunoprecipitation and Immunodetection of Natural IgG

The same volumes of serum and protein G sepharose (slurry 1:1) were mixed together and incubated for 1 hour at 4°C under constant agitation. Pellets were collected by centrifuging at 10,000*g* at 4°C and were resuspended in 2× Laemmli buffer. Samples were boiled for 5 minutes and were centrifuged; supernatants were analyzed by immunoblot analysis as described above. In some experiments, accumulation of natural IgG was evaluated in tumor sections using an Alexa Fluor 488 antimouse IgG.

Flow Cytometry Analysis

Blood samples were freshly collected, and red blood cells were eliminated by centrifugation on Histopaque 1083 (Sigma). Cells were then labeled with a biotin-conjugated monoclonal antibody from BD Pharmingen (anti-B220, clone RA3-6B2) then with PE-conjugated streptavidin. Fluorescence signals were measured using a FACScan apparatus (BD Pharmingen) and analyzed by the FlowJo software (Tree Star, Inc, Olten, Switzerland).

Statistical Analysis

Data are expressed as means ± SEM or as scatter plots. Student's *t* test and one-way analysis of variance were used where appropriate.

Results

SERPA Identification of GRP78 Auto-Abs in Tumor-Bearing Mice

Total proteins extracted from LLc tumors were separated by two-dimensional PAGE and were transferred onto PVDF membranes. Pooled sera from tumor-bearing mice and control mice (n = 15 per condition) were probed separately for the presence of auto-Abs directed against tumor proteins. Multiplexing analysis was performed taking advantage of the Cy5 prelabeling of tumor proteins and the detection of the anti-IgG peroxidase-conjugated secondary antibody in the Cy2 wavelength (Figure W1). The long-lasting and stable chemiluminescence from the ECL Plus reagent used in our experiments gave a stable fluorescence signal. The low interindividual variability in this mouse tumor model led to the identification of 40 serum-labeled spots on the two-dimensional blots. The proteins of interest were excised from preparative gels and digested with trypsin, and the peptide mixtures were analyzed by mass spectrometry. This led to the identification of 24 proteins with satisfying scores (Table W1), among which 12 were tumor-bearing mouse serum–positive (Table 1). Only four antigens, however, were exclusively recognized by the serum of tumor-bearing mice: GRP78, aldolase A1, vinculin, and heterogeneous nuclear ribonucleoprotein L. In the rest of the study, we chose to focus on GRP78 (also called BiP), which was the antigen giving the strongest immunoblot signal (see enlarged spot in Figure 1).

GRP78 Autoantigen Validation

The GRP78 identification was confirmed by probing two-dimensional membranes with commercially available anti-GRP78 antibody (Figure 2*A*). We then examined by Western blot analysis the GRP78 expression level in LLc tumor cells and found that it amounted to more than five-fold the abundance in the host tissue (Figure 2*B*). Furthermore, while in the host tissue, GRP78 was exclusively found intracellularly in agreement with its endoplasmic reticulum (ER) function; immunohistochemistry revealed that, in

Table 1. List of Identified Tumor Proteins Detected by Two-dimensional Immunoblot Analysis with the Sera of Tumor-Bearing Mice

Proteins	p*I*	MW (kDa)	Mascot Score	Uniprot no.	Queries Matched	Sequence Coverage (%)	*P* (Expect)
MALDI identification							
inner membrane protein mitochondrial cra	6.18	83	148	Q8CAQ8	34	52	1.81e–12
Villin 2	5.83	69	245	P26040	41	60	4.50e–20
Grp78	4.79	72	240	P20029	36	56	1.40e–19
Heat shock protein 1	4.93	84	125	P07901	29	51	1.80e–08
Heterogeneous nuclear ribonucleoprotein l	6.07	70	161	Q499X2	22	47	5.70e–13
Heterogeneous nuclear ribonucleoprotein k	5.39	51	119	P61979	18	41	1.80e–07
Vimentin	4.77	52	225	P20152	31	59	4.50e–18
Lap 3	7.61	56	153	Q9CPY7	27	56	1.10e–10
Lectin, galactose binding, soluble 3	8.50	30	122	P16110	9	80	9.10e–08
QTOF identification							
Aldolase 1, A isoform	8.40	40	471	P05064	7		
Procollagen lysine, 2-oxoglutarate 5-dioxygenase 3	5.81	85	389	Q9R0E1	4		
Vinculin	5.88	117	1160	Q64727	16		

tumor cells, GRP78 was aberrantly located at the plasma membrane (Figure 2*C*).

GRP78 Auto-Abs as a Marker of Tumor Growth

An ELISA was developed using recombinant GRP78 protein to confirm the presence of auto-Abs in the serum of tumor-bearing mice and to track titer changes in response to treatments. Calibration was carried out for each ELISA assay, and a linear relationship was consistently observed in the range of antibody concentration detected from the mouse serum (Figure W2). Blood was collected from tumor-bearing mice on days 0, 3, 7, 10, 14, and 17 after injection (intramuscular) with 10^6 tumor cells. ELISA revealed that a net increase in GRP78 auto-Abs was detectable in the tumor-bearing mouse serum as soon as 3 days after tumor cell injection. Interestingly, at that early time, tumor growth, as measured with an electronic caliper, was not yet detectable; tumors were actually palpable from day 7 (Figure 3*B*). GRP78 auto-Ab signal remained stable from day 3 to day 7 after injection but peaked on day 10; values detected on days 14 and 17 were barely higher than those observed on day 7. Because day 10 is usually the time required for angiogenesis to become functional, we examined the difference in endothelial staining using anti-CD31 antibody and blood flow around this period. We confirmed a significant increase in large, mature blood vessels on day 14 *versus* a punctate, angiogenic pattern on day 7 (Figure 3*E*). A dramatic increase in tumor blood flow was also observed between day 7 and day 14, as determined using laser Doppler imaging (Figure 3*F*).

In other series of animals aimed to examine the effect of metastases spreading on the anti-GRP78 titer, we stimulated the development of dormant lung metastases by surgically removing the primary tumor (when reaching 8 mm in diameter), as previously documented in this tumor model [16]. Interestingly, whereas a net increase in anti-GRP78 antibody was observed 9 days after surgery (Figure 3*C*), the detection of metastases required 5 to 10 more days (see day 14 [6/9 mice] and day 19 in Figure 3*D*). Between day 14 and day 19,

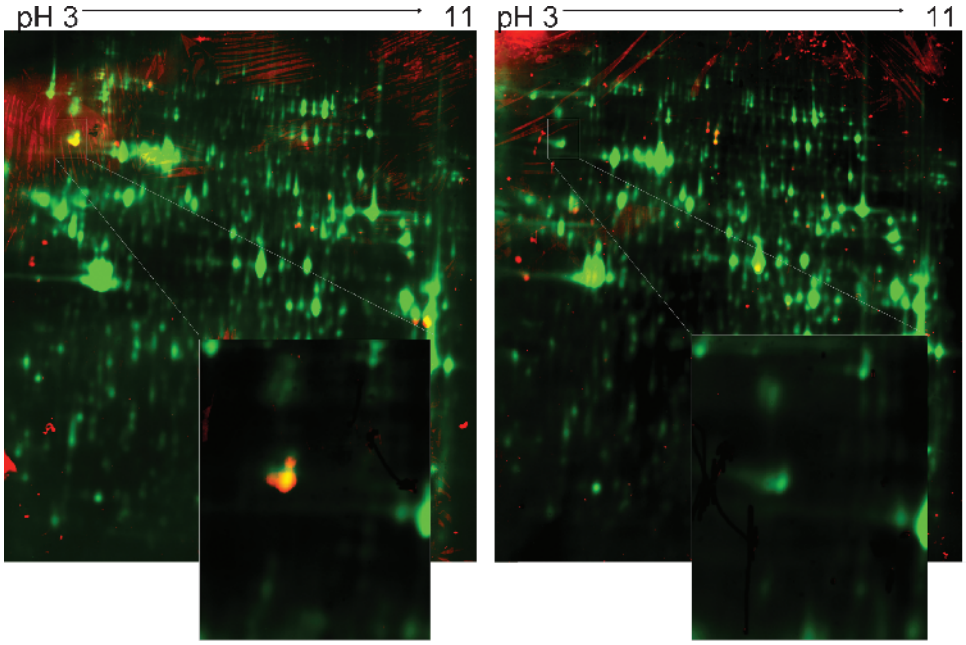

Figure 1. SERPA of LLc tumor-bearing mice. Representative immunoblot analysis with pooled sera from tumor-bearing mice (left panel) or control mice (right panel) ($n = 15$) on Cy5-labeled LLc tumor extracts; yellow/red spots correspond to proteins recognized by auto-Ab present in the sera. This experiment was repeated four times; the enlarged spot corresponds to GRP78, as confirmed after picking, trypsin digestion, and consecutive MALDI identification.

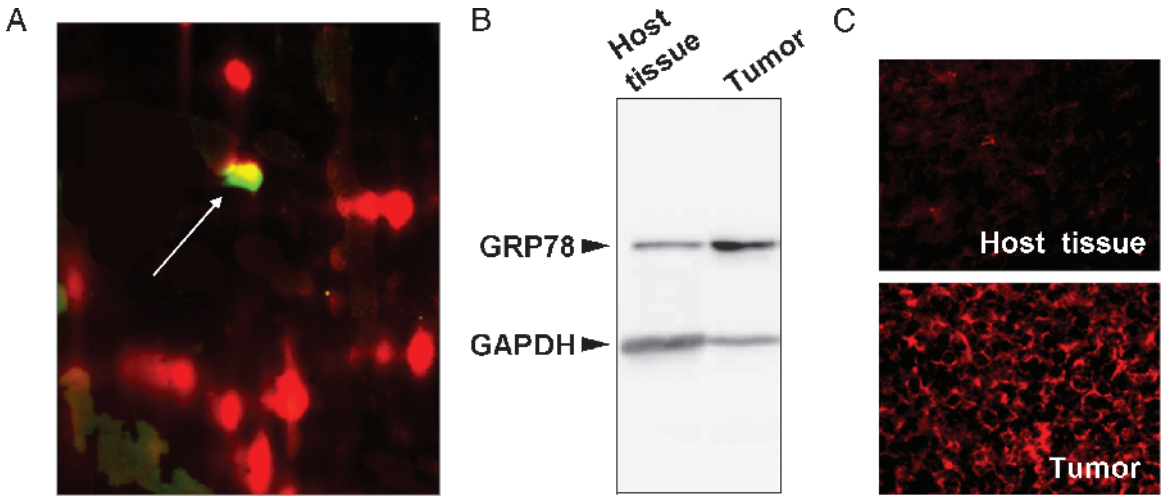

Figure 2. Validation of GRP78 as a tumor autoantigen. (A) Immunoblot analysis with commercial anti-GRP78 of the putative GRP78 spot from LLc tumor extracts separated on two-dimensional membranes. (B) Representative Western blot analysis of the expression of GRP78 in host tissue and tumors (n = 4); simultaneous glyceraldehyde-3-phosphate dehydrogenase (GAPDH) immunoblot analysis was used as a control. (C) Representative GRP78 immunostaining on host tissue (top) and tumor (bottom) sections; immunostaining experiments were repeated several times with similar results.

more than 50% of the mice died because of lung metastases. Interestingly, among the mice alive on day 19, the anti-GRP78 levels were usually in the low percentile range (Figure 3*C*).

Effect of Radiotherapy and Chemotherapy on GRP78 Auto-Ab Titer

To study the effect of treatments on the expression of GRP78 auto-Abs, we chose radiotherapy and chemotherapy regimens. Accordingly, tumor-bearing mice were exposed to 16-Gy radiation, 100-mg/kg cyclophosphamide administered intraperitoneally (bolus, two injections at 5-day interval), or low-dose cyclophosphamide in the drinking water (so-called *metronomic chemotherapy*). Radiotherapy and bolus cyclophosphamide are known to exert profound antitumor effects, as confirmed in Figure 4, *A* and *C*, respectively. Metronomic cyclophosphamide therapy is a therapeutic scheme proposed to have a better benefit/toxicity balance than the conventional maximal tolerated dose regimen [15]. In this study, we observed an initial response of the tumor to metronomic cyclophosphamide but a loss of efficacy on the longer term (Figure 4*E*). ELISA revealed that radiotherapy led to an increase in circulating anti-GRP78, peaking at five-fold the level observed 5 days before the radiation exposure (Figure 4*B*). Of note, local irradiation of control animals (ie, without tumor) failed to lead to any changes in anti-GRP78 concentrations (not shown). Chemotherapy gave rise to an opposite pattern, with a significant reduction of anti-GRP78 auto-Ab concentration (Figure 4, *D* and *F*). Note the continuous decrease in anti-GRP78 auto-Ab with metronomic chemotherapy despite the lesser inhibitory effect of this drug regimen on tumor growth (Figure 4*F*).

Immune Response Toward the Different Treatments

To understand the reasons of the decrease in anti-GRP78 auto-Ab after chemotherapy, we evaluated whether the systemic cytotoxic effects of cyclophosphamide could influence the humoral response by antibody-producing lymphocytes. We therefore used flow cytometry to evaluate potential changes in the extent of B cells in treated *versus* untreated tumor-bearing mice (Figure 5*A*). We observed that, whereas radiotherapy did not alter the amounts of B-220–positive B cells, cyclophosphamide administration led to a 20% to 50% reduction in B cells (Figure 5*B*). The reduction in B-cell numbers after chemotherapy did correlate with a reduction in the extent of circulating IgG as determined by immunoprecipitation from cyclophosphamide-exposed mouse sera (Figure 5*C*). Because radiotherapy led to a similar reduction in circulating IgG despite a maintained amount of B cells, we further examined whether antibodies could be trapped into the irradiated tumor. Figure 5*D* shows that the overall detection of IgG from tumor sections was indeed significantly increased in response to radiotherapy (*vs* untreated tumors, n = 5). Immunohistochemical analysis of the same tumor sections further revealed that GRP78 expression was also dramatically increased in irradiated tumors (Figure 5*D*).

Discussion

The major findings of this study are that (i) increase in circulating anti-GRP78 auto-Ab is associated with the detection of primary tumor and metastases at earlier times than with palpation and microscopic analysis of the invaded tissues, respectively; (ii) chemotherapy and radiotherapy have opposite effects on the extent of circulating anti-GRP78 auto-Ab, prompting caution in interpreting changes in auto-Ab titers in response to anticancer treatments; and (iii) Cy-dyes multiplex analysis may optimize the SERPA workflow.

An increasing number of studies report the identification of auto-Ab in cancer patients as potential new biomarkers for cancer detection and prognosis [1–14]. Although several good candidates are making their route toward validation in larger studies, a variable proportion of patients with a given cancer type are usually positive for the considered auto-Ab. Most of these studies aiming to identify auto-Ab as new cancer biomarkers are carried out by comparing the sera of cancer patients with the sera of healthy volunteers or patients with cancer-predisposing diseases (eg, polyps, cirrhosis, viral infection). The status of patients at the time of the serum collection is therefore variable, and the influence of treatments (targeting cancer or precancerous lesions) is rarely integrated in the interpretation of the results. Another related issue is the potential and reliability of auto-Ab–based markers to follow the response to treatments. From a theoretical point of view,

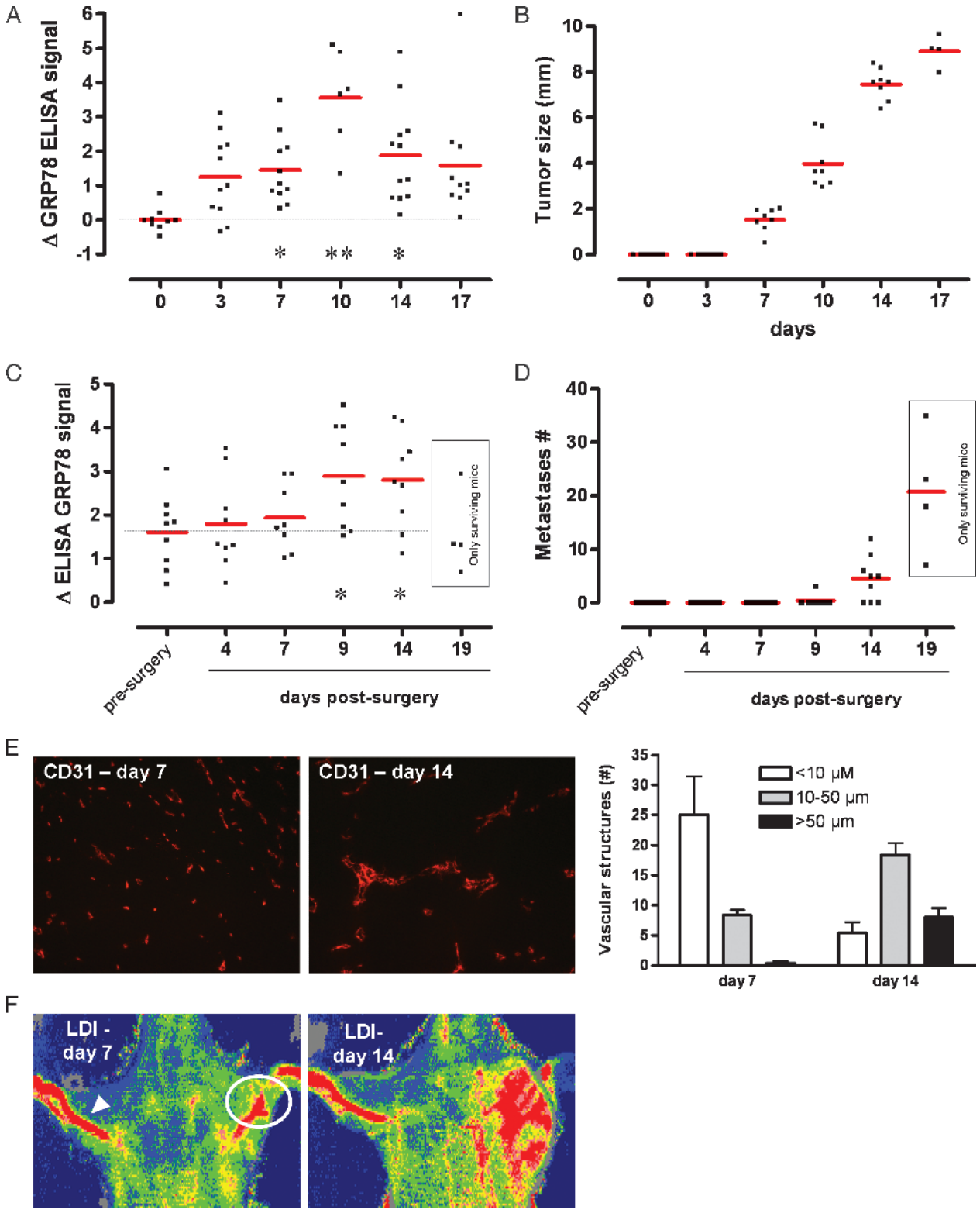

Figure 3. Changes in the titer of anti-GRP78 auto-Ab as a marker of primary tumor growth and metastases. (A) GRP78-specific ELISA was performed from sera collected through retro-orbital bleeding of mice before (day 0) and after (days 3, 7, 10, 14, and 17) tumor cell injection. Results are presented as scatter plots; $*P < .05$, $**P < .01$. (B) Tumor diameters as measured with a caliper. (C) GRP78-specific ELISA was performed at the indicated time after primary tumor removal to activate lung metastases. Results are presented as scatter plots; $*P < .05$. (D) Number of lung metastases identified by histologic analysis of lungs collected from tumor-bearing mice at the indicated time before and after surgery. Note that on day 19 in panels C and D, only data arising from surviving animals are presented. (E) Representative CD31 immunostaining of tumor sections on days 7 and 14. Histogram represents the distribution of CD31-positive vascular structures according the indicated sizes. (F) Representative laser Doppler imaging (LDI) pictures from LLc tumor-bearing mice on days 7 and 14 after injection of tumor cells. The average perfusions of the tumor-bearing leg (white circle) and of the control leg (arrowhead) can be evaluated on the basis of the colored histogram pixels.

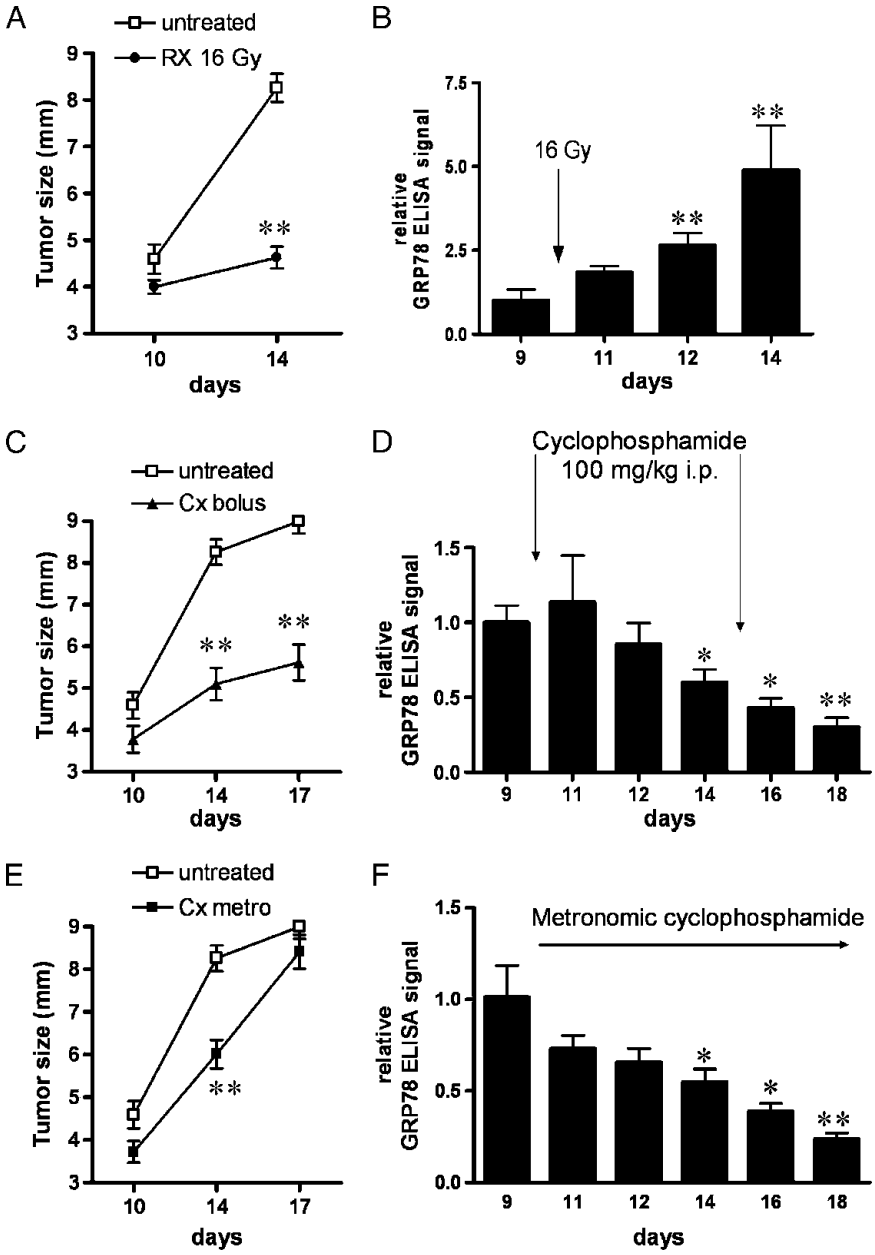

Figure 4. Differential influence of radiotherapy and chemotherapy on GRP78 auto-Abs titer. Changes in tumor growth and seric GRP78 auto-Ab signal (detected by ELISA) observed after radiotherapy, or cyclophosphamide under bolus (100 mg/kg intraperitoneally) or metronomic (through the drinking water) administrations. Panels A, C, and E show the effects of either treatment on tumor growth; $^{**}P < .01$ *versus* day 10. Bar graphs represent the effects of either treatment on GRP78 auto-Ab signal from tumor-bearing (B, D, and F). $^{*}P < .05$, $^{**}P < .01$ *versus* day 9 (before treatment administration).

eradication of a tumor should lead to a decrease in TAAs and thus in the corresponding circulating auto-Ab.

Here, we used a mouse tumor model to work with a more condensed process of tumor growth and consecutive metastatic spreading than what is observed in the course of the disease in humans. Such an animal model also allows to reduce the interindividual variability observed with patients. A multiplex analysis was further applied to optimize the detection of auto-Ab, through the coregistration of the Cy5 staining of tumor cell proteins separated on two-dimensional gels and the Cy2-channel detection of the ECL-driven chemiluminescence from the peroxidase-conjugated secondary antibody. This multiplex strategy, which advantageously replaced the conventional approach matching the immunoblot with Coomassie blue– or silver-stained gels, led us to identify a rather limited number of spots. From the short list of proteins selectively recognized by the sera of tumor-bearing mice, we have selected GRP78 (ie, the highest immune signal after serum immunoblot analysis) to address the issues of changes in auto-Ab titer with metastatic spreading and treatments.

GRP78, a member of the heat shock protein 70 family, plays key roles in the ER stress response [17]. In tumor cells, ER stress is a common phenomenon observed in response to nutrient deprivation, acidosis, or hypoxia [18]. In these hostile conditions, GRP78 facilitates proper protein folding and targets misfolded protein for proteasome degradation [18,19]. Shedding of GRP78 protein was reported to sign the presence of cancer [18] and a recent study identified critical roles of GRP78 in tumor cell survival and angiogenesis [19].

Interestingly, anti-GRP78 auto-Abs were recently identified as biomarkers of the clinical progression of prostate [20,21] and ovarian cancers [22]. In these human studies, serum reactivity against GRP78 correlated positively with natural cancer progression, allowing to discriminate between organ-confined, locally advanced, and metastatic prostate cancers [20] and between early stages and stages III/IV of ovarian cancer [21]. The choice of anti-GRP78 as a generic auto-Ab detected in our mouse tumor model is therefore supported by clinical data validating this marker of cancer progression. In our study, the immunogenicity of GRP78 is likely to find its origin in the overexpression and the mislocalization of GRP78 at the plasma membrane of tumor cells (Figure 2). Importantly, we showed that anti-GRP78 auto-Ab was detected in the serum of mice well before the detection of the tumor by palpation or caliper measurements (Figure 3, *A* and *B*).

Taking advantage of the induction of dormant lung metastases after the removal of the primary tumor [16], we showed that an increase in anti-GRP78 auto-Ab concentrations was detectable at a time when microscopic evaluation of the lungs failed to identify metastases (Figure 3, *C* and *D*). These results give credential to the use of anti-GRP78 antibody as early biomarkers of both primary tumor emergence and activation of dormant metastases after surgery. We found, however, that the titer of circulating anti-GRP78 auto-Ab did not increase linearly with the tumor burden (Figure 3, *A* and *B*). In particular, the onset of a functional vascularization in the tumor (Figure 3, *E* and *F*) was associated with an acute increase in auto-Ab detection (see day 10 in Figure 3*A*).

The data establishing GRP78 as a key immunogenic protein in our tumor model led us to evaluate whether anti-GRP78 auto-Ab could also be exploited as a marker of the response to radiotherapy and chemotherapy. Although we used a 16-Gy irradiation and bolus cyclophosphamide that inhibited tumor growth to the same extent (Figure 4, *A* and *C*), we found that chemotherapy administration was associated with a reduction in the serum titer of anti-GRP78 antibodies, whereas radiotherapy increased it (Figure 4, *B* and *D*).

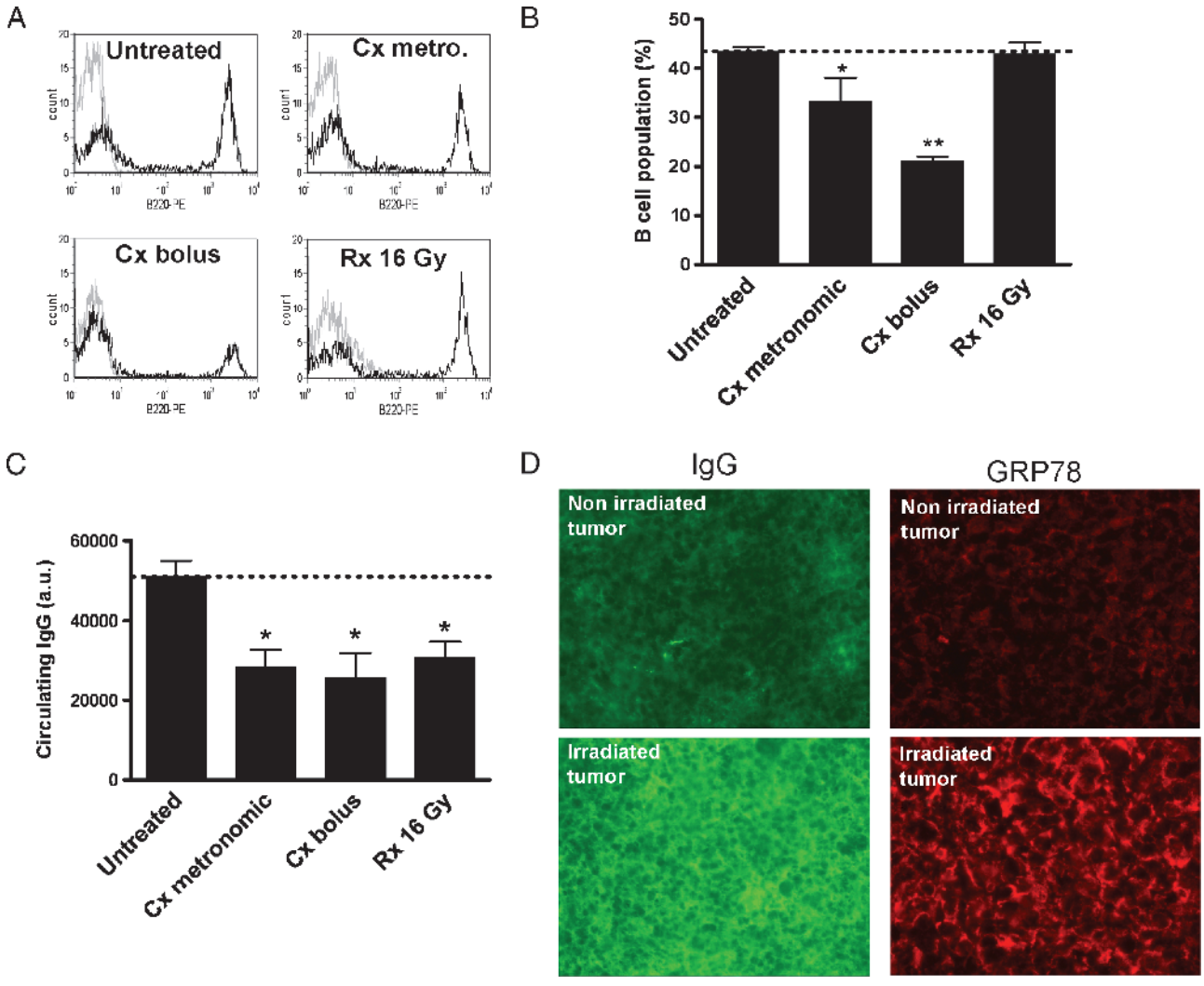

Figure 5. Humoral immune responses of tumor-bearing mice to radiotherapy or chemotherapy. B-cell number determination from the blood of control or treated tumor-bearing mice (see Figure 4 legend for treatment details): representative flow cytometry analyses of B220-expressing blood cells (A) and quantification (B) are presented; $^*P < .05$, $^{**}P < .01$ ($n = 3$). (C) Changes in the total amounts of circulating IgG were also determined after immunoprecipitation from the blood of tumor-bearing mice; $^*P < .05$ ($n = 3$). (D) Representative pictures of immunohistochemical analyses of tumor sections documenting the trapping of IgG (left) or the extent of GRP78 protein expression (right) in nonirradiated (top) or irradiated (bottom) tumors. These experiments were repeated on five different tumors per condition with similar results; staining and optic conditions were strictly identical between untreated and irradiated tumors.

We found that the decrease in anti-GRP78 auto-Ab (and circulating Ig in general) after cyclophosphamide administration could be related to the observed net reduction in lymphocytes, in particular the antibody-producing B-cell population (Figure 5, *A* and *B*). Moreover, the metronomic scheme of cyclophosphamide administration used in this study, although less efficient in inhibiting tumor growth, did not spare the anti-GRP78 titer, which also decreased with time (Figure 4*F*). Altogether, these observations stress that myelotoxic treatments, as observed with most chemotherapeutic strategies [23–25], could be misguiding by inadequately linking reductions in tumor biomarker concentrations and in tumor mass.

In contrast, as anticipated, local irradiation of the tumor did not influence the number of B cells in treated animals. The observed radiation-driven increase in anti-GRP78 auto-Ab may instead be related to an overall increased stress response favoring the expression of functional GRP78 (as shown in Figure 5*D*); additional mechanisms could involve radiation-triggered degradation of GRP78 protein, thereby increasing the pool of peptides presented by the MHC class I pathway. The observed local increase in IgG abundance in the tumor (Figure 5*D*) and the overall decrease in circulating IgG after radiation (Figure 5*C*) support this hypothesis of an overall stimulated immune response. Also, the response was tumor-selective because we did not observe any increase in anti-GRP78 auto-Ab by irradiating the host tissue (in non–tumor-bearing mice; not shown). Together with the observation that, in response to radiotherapy, the circulating anti-GRP78 auto-Ab titer increased despite the overall decrease in circulating antibodies (Figures 4*B* and 5*C*), our data confirm that GRP78 is one of the key protein against which an immune response is mounted in tumors.

In conclusion, we identified the anti-GRP78 auto-Ab as an early seric marker of tumor and metastatic progression and showed how its titer may be differently influenced by radiotherapy and chemotherapy. Although not excluding the use of auto-Ab as markers of response to conventional anticancer treatments, this study with an archetypical auto-Ab emphasizes the need to integrate factors such as B cells' depletion or promotion of the antigen-presenting process to interpret the data. Our study therefore brings new insights in the process of identifying new biomarkers from the serological proteome by (i) drawing the attention to the therapeutic status of cancer patients recruited in studies aiming to identify new auto-Abs as cancer biomarkers and (ii) reporting the integration of CyDyes multiplex technology as a way to improve SERPA-based detection of tumor auto-Abs.

References

[1] Caron M, Choquet-Kastylevsky G, and Joubert-Caron R (2007). Cancer immunomics using autoantibody signatures for biomarker discovery. *Mol Cell Proteomics* **6**, 1115–1122.

[2] Desmetz C, Cortijo C, Mange A, and Solassol J (2009). Humoral response to cancer as a tool for biomarker discovery. *J Proteomics* **72**, 982–988.

[3] Zhang JY, Megliorino R, Peng XX, Tan EM, Chen Y, and Chan EK (2007). Antibody detection using tumor-associated antigen mini-array in immunodiagnosing human hepatocellular carcinoma. *J Hepatol* **46**, 107–114.

[4] Tan EM and Zhang J (2008). Autoantibodies to tumor-associated antigens: reporters from the immune system. *Immunol Rev* **222**, 328–340.

[5] Lu H, Goodell V, and Disis ML (2008). Humoral immunity directed against tumor-associated antigens as potential biomarkers for the early diagnosis of cancer. *J Proteome Res* **7**, 1388–1394.

[6] Ludwig N, Keller A, Heisel S, Leidinger P, Klein V, Rheinheimer S, Andres CU, Stephan B, Steudel WI, Graf NM, et al. (2009). Improving seroreactivity-based detection of glioma. *Neoplasia* **11**, 1383–1389.

[7] Banks RE, Craven RA, Harnden P, Madaan S, Joyce A, and Selby PJ (2007). Key clinical issues in renal cancer: a challenge for proteomics. *World J Urol* **25**, 537–556.

[8] Hardouin J, Lasserre JP, Sylvius L, Joubert-Caron R, and Caron M (2007). Cancer immunomics: from serological proteome analysis to multiple affinity protein profiling. *Ann N Y Acad Sci* **1107**, 223–230.

[9] Tan HT, Low J, Lim SG, and Chung MC (2009). Serum autoantibodies as biomarkers for early cancer detection. *FEBS J* **276**, 6880–6904.

[10] Kijanka G and Murphy D (2009). Protein arrays as tools for serum autoantibody marker discovery in cancer. *J Proteomics* **72**, 936–944.

[11] De Monte L, Sanvito F, Olivieri S, Vigano F, Doglioni C, Frasson M, Braga M, Bachi A, Dellabona P, Protti MP, et al. (2008). Serological immunoreactivity against colon cancer proteome varies upon disease progression. *J Proteome Res* **7**, 504–514.

[12] Ran Y, Hu H, Zhou Z, Yu L, Sun L, Pan J, Liu J, and Yang Z (2008). Profiling tumor-associated autoantibodies for the detection of colon cancer. *Clin Cancer Res* **14**, 2696–2700.

[13] Qiu J, Choi G, Li L, Wang H, Pitteri SJ, Pereira-Faca SR, Krasnoselsky AL, Randolph TW, Omenn GS, Edelstein C, et al. (2008). Occurrence of autoantibodies to annexin I, 14-3-3 theta and LAMR1 in prediagnostic lung cancer sera. *J Clin Oncol* **26**, 5060–5066.

[14] Desmetz C, Bascoul-Mollevi C, Rochaix P, Lamy PJ, Kramar A, Rouanet P, Maudelonde T, Mange A, and Solassol J (2009). Identification of a new panel of serum autoantibodies associated with the presence of *in situ* carcinoma of the breast in younger women. *Clin Cancer Res* **15**, 4733–4741.

[15] Man S, Bocci G, Francia G, Green SK, Jothy S, Hanahan D, Bohlen P, Hicklin DJ, Bergers G, and Kerbel RS (2002). Antitumor effects in mice of low-dose (metronomic) cyclophosphamide administered continuously through the drinking water. *Cancer Res* **62**, 2731–2735.

[16] O'Reilly MS, Holmgren L, Shing Y, Chen C, Rosenthal RA, Moses M, Lane WS, Cao Y, Sage EH, and Folkman J (1994). Angiostatin: a novel angiogenesis inhibitor that mediates the suppression of metastases by a Lewis lung carcinoma. *Cell* **79**, 315–328.

[17] Melnick J and Argon Y (1995). Molecular chaperones and the biosynthesis of antigen receptors. *Immunol Today* **16**, 243–250.

[18] Lee AS (2007). GRP78 induction in cancer: therapeutic and prognostic implications. *Cancer Res* **67**, 3496–3499.

[19] Dong D, Ni M, Li J, Xiong S, Ye W, Virrey JJ, Mao C, Ye R, Wang M, Pen L, et al. (2008). Critical role of the stress chaperone GRP78/BiP in tumor proliferation, survival, and tumor angiogenesis in transgene-induced mammary tumor development. *Cancer Res* **68**, 498–505.

[20] Mintz PJ, Kim J, Do KA, Wang X, Zinner RG, Cristofanilli M, Arap MA, Hong WK, Troncoso P, Logothetis CJ, et al. (2003). Fingerprinting the circulating repertoire of antibodies from cancer patients. *Nat Biotechnol* **21**, 57–63.

[21] Gonzalez-Gronow M, Cuchacovich M, Llanos C, Urzua C, Gawdi G, and Pizzo SV (2006). Prostate cancer cell proliferation *in vitro* is modulated by antibodies against glucose-regulated protein 78 isolated from patient serum. *Cancer Res* **66**, 11424–11431.

[22] Taylor DD, Gercel-Taylor C, and Parker LP (2009). Patient-derived tumor-reactive antibodies as diagnostic markers for ovarian cancer. *Gynecol Oncol* **115**, 112–120.

[23] Machiels JP, Reilly RT, Emens LA, Ercolini AM, Lei RY, Weintraub D, Okoye FI, and Jaffee EM (2001). Cyclophosphamide, doxorubicin, and paclitaxel enhance the antitumor immune response of granulocyte/macrophage-colony stimulating factor–secreting whole-cell vaccines in HER-2/*neu* tolerized mice. *Cancer Res* **61**, 3689–3697.

[24] Zitvogel L, Apetoh L, Ghiringhelli F, and Kroemer G (2008). Immunological aspects of cancer chemotherapy. *Nat Rev Immunol* **8**, 59–73.

[25] Zitvogel L, Apetoh L, Ghiringhelli F, Andre F, Tesniere A, and Kroemer G (2008). The anticancer immune response: indispensable for therapeutic success? *J Clin Invest* **118**, 1991–2001.

Supplementary Data

Materials and Methods

MALDI identification. Peptides digest were desalted on C18 Geloader pipette Tips (Proxeon Biosystems, Odense, Denmark) and directly eluted on the target with a mix (1:1 vol./vol.) of α-cyano-4-hydroxyciannamic acid (in 7:3 vol./vol. acetonitrile/5% formic acid) and 2,5-dihydroxybenzoic acid (in 7:3 vol./vol. acetonitrile/0.1% trifluoracetic acid). Peptide mass fingerprints were obtained using a MALDI-MX mass spectrometer (Walters). ProteinLynx Global Server 2.2.5 (Waters) was used as a peak list–generating software. Two external calibrations were used: lock mass with ADH digest and lock mass with 1618.84 Da. The trypsin autodigestion peak at 2211.1046 Da was used for the internal calibration. In-house Mascot 2.2 server was used as database search engine; PMF search was performed on *Mus musculus* subset of the National Center for Biotechnology Information nonredundant database (NCBInr; 138,000 entries in 2008 sequences). Parameters for peptide matching were a peptide tolerance of 100 ppm, a maximum of one missed cleavage, carbamidomethylation was allowed as a fixed modification, and oxidation of methionine was allowed as a variable modification. For all protein identifications, a minimal individual score of 64 (identity score) and expect value less than 1 were used for the identification criteria.

QTOF identification. Peptides were analyzed by using a nanoflow liquid chromatography coupled to tandem mass spectrometry with electrospray ionization. (Waters) instrument on a CapLC Q-TOF2 mass spectrometer (Waters). The digests were separated by reverse-phase liquid chromatography using a 75-μm × 150-mm reverse-phase NanoEase column (Waters) in a CapLC (Waters) liquid chromatography system. Mobile phase A was 95% of 0.1% formic acid in water and 5% acetonitrile. Mobile phase B was 0.1% formic acid in acetonitrile. The digest (1 μl) was injected, and the organic content of the mobile phase was increased linearly from 5% to 40% B in 40 minutes and from 40% to 100% B in 5 minutes. The column effluent was connected to a PicoTip emitter (New Objective, Woburn, MA) inside the Q-TOF source. Peptides were analyzed in data-dependent acquisition mode on a Q-TOF2 (Waters) instrument. In a survey scan, MS spectra were acquired for 1 second in the *m/z* range between 450 and 1500. For MS/MS raw data, peak lists were created using Distiller (Matrix Sciences), and in-house Mascot 2.2 (Matrix Sciences) server was used as database search engine. Enzyme specificity was set to trypsin, and the maximum number of missed cleavages per peptide was set at 1. Carbamidomethylation was allowed as a fixed modification, and oxidation of methionine was allowed as a variable modification. Mass tolerance for the monoisotopic precursor peptide window and MS/MS tolerance window were set to ±0.3 Da. We also specified ESI-Q-TOF as an instrument. The peak lists were searched against the *Mus musculus* subset of the National Center for Biotechnology Information nonredundant (NCBInr) database (138,000 entries in 2008). Control searches of all the files against the whole NCBInr database (5,454,477 entries in 2008) were used to confirm the identification. For all protein identifications in MS/MS, a minimal individual peptide score of 36 (if less than this score, no identity or homology was found for the analyzed peptides) and expect value less than 1 were used for the initial identification criteria. Moreover, the correlation between theoretical p*I* and molecular mass of the protein with the position of the corresponding spot in the two-dimensional gel was also taken into account.

Results

We identified 40 serum-labeled spots on the two-dimensional blots. The proteins of interest were excised from preparative gels and digested with trypsin, and the peptide mixtures were analyzed by MS. This led to the identification of 24 different proteins with satisfying scores (see criteria; Table W1), among which 12 were recognized by pooled sera of tumor-bearing mice. The extensive data sets corresponding to the identification of the tumor serum–positive antigens are provided in Table W2.

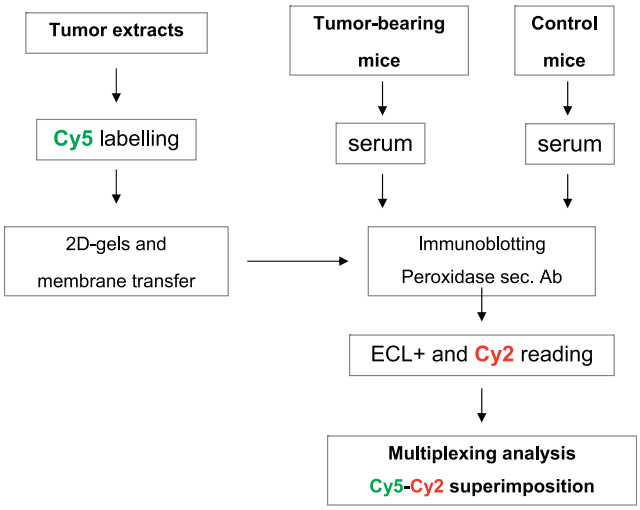

Figure W1. Schematic overview of the multiplex-based detection of auto-Ab. Cy5-labeling of tumor extracts is coregistered with enhanced chemiluminescence (ECL)–based detection of the peroxidase-conjugated secondary antibody using the Cy2 channel detection.

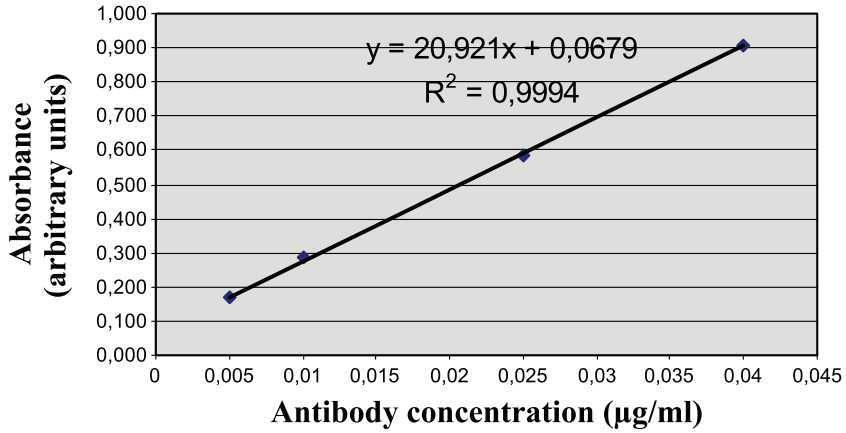

Figure W2. Representative anti-GRP78 ELISA calibration. The 96-well plates coated with 5 μg/ml recombinant GRP78 protein (Stressgen) were used. Specific hybridization using serial dilutions of GRP78 antibody (BD Pharmingen) was measured with a peroxidase-conjugated antimouse IgG antibody (dilution, 1:10,000) and addition of 3,3′,5,5′-tetramethylbenzidine (Calbiochem). Plates were read at 450 nm in a VictorX4 microplate reader.

Table W1. List of Identified Tumor Proteins Detected by Two-dimensional Immunoblot Analysis with the Sera of Control and/or Tumor-Bearing Mice.

	Proteins Recognized by Control Mouse Serum	Proteins Recognized by Tumor-Bearing Mouse Serum
Inner membrane protein mitochondrial, isoform CRA_a and b	+	+
Villin 2	+	+
Glucose-regulated protein GRP78		+
Sorting-nexin 9	+	
Heat shock protein 1	+	+
Heterogeneous nuclear ribonucleoprotein L		+
Heterogeneous nuclear ribonucleoprotein K	+	
Lamin A/C	+	
Septin 11	+	
Vimentin	+	+
Lap 3	+	+
Similar to actin	+	
Pyrophosphatase	+	
Lectin, galactose binding, soluble 3	+	+
Alanyl-tRNA synthetase	+	
Ubiquitin specific protease 5 (isopeptidase T)	+	
Aldolase 1, A isoform		+
gamma-Actin	+	
Annexin A11	+	
Heat shock protein HSP 90-beta Hsp 84	+	
Procollagen-lysine, 2-oxoglutarate 5-dioxygenase 3	+	+
Protein 40 kDa	+	+
Gelsolin-like capping protein	+	
Vinculin		+

Table W2. List of Tumor Antigens and Related Digested Peptides Identified on the Basis of Their Mass Fingerprint.

inner membrane protein, mitochondrial, isoform CRA_a and CRA_b

Score: **169** Expect: **1.8e-012**

Number of unique mass values matched: **34**
Sequence Coverage: **52%**

Start - End	Observed	Mr(expt)	Mr(calc)	ppm	Miss	Sequence
85 - 101	1805.9049	1804.8976	1804.9797	-45	0	K.LFGMVLGSAPYTVPLPK.K Oxidation (M)
102 - 110	953.5324	952.5251	952.5706	-48	0	K.KPVQSGPLK.I
131 - 158	2777.3716	2776.3643	2776.3879	-9	1	K.TKGDTPASAAGDTLSVPAPAVQHEDTIK.T
169 - 183	1617.7565	1616.7492	1616.7166	20	0	K.STSETTEEAFSSSVR.E
184 - 193	1153.6104	1152.6031	1152.5887	13	0	R.ERPPEEVAAR.L
219 - 238	2031.1125	2030.1052	2030.1008	2	0	R.TSSVTLQTITAQNAAVQAVK.A
293 - 301	1064.5860	1063.5787	1063.5583	19	1	K.MKTIIEDAK.K Oxidation (M)
295 - 302	917.4857	916.4784	916.5229	-49	1	K.TIIEDAKK.R
304 - 318	1493.7893	1492.7820	1492.7634	12	0	R.EIAGATPHITAAEGR.L
319 - 331	1509.7992	1508.7919	1508.8021	-7	0	R.LHNMIVDLDNVVK.K
319 - 331	1525.8120	1524.8047	1524.7970	5	0	R.LHNMIVDLDNVVK.K Oxidation (M)
319 - 332	1653.8451	1652.8378	1652.8920	-33	1	R.LHNMIVDLDNVVKK.V Oxidation (M)
342 - 354	1527.8447	1526.8374	1526.8205	11	0	K.VVSQYHELVVQAR.D
359 - 373	1699.8602	1698.8529	1698.8828	-18	1	R.KELDSITPDITPGWK.G
360 - 373	1571.7997	1570.7924	1570.7879	3	0	K.ELDSITPDITPGWK.G
360 - 378	2046.0180	2045.0107	2045.0139	-2	1	K.ELDSITPDITPGWKGMTGK.L
379 - 393	1662.8756	1661.8683	1661.8485	12	0	K.LSTDDLNSLIAHAHR.R
394 - 400	914.5229	913.5156	913.5093	7	1	R.RIDQLNR.E
411 - 419	1080.6227	1079.6154	1079.5975	17	0	K.QHIELALEK.H
469 - 478	1119.5969	1118.5896	1118.5581	28	0	R.QAAAHTDHLR.D
490 - 499	1229.6070	1228.5997	1228.5612	31	0	K.YEFEQGLSEK.L
500 - 508	1150.6001	1149.5928	1149.5666	23	0	K.LSEQELEFR.R
500 - 509	1306.6755	1305.6682	1305.6677	0	1	K.LSEQELEFRR.R
511 - 528	2089.9753	2088.9680	2088.9422	12	0	R.SQEQMDSFTLDINTAYAR.L
511 - 528	2105.9668	2104.9595	2104.9371	11	0	R.SQEQMDSFTLDINTAYAR.L Oxidation (M)
531 - 547	1823.9110	1822.9037	1822.8809	13	0	R.GIEQAVQSHAVAEEEAR.K
531 - 548	1951.9814	1950.9741	1950.9759	-1	1	R.GIEQAVQSHAVAEEEARK.A
548 - 560	1522.8652	1521.8579	1521.8667	-6	1	R.KAHQLWLSVEALK.Y
549 - 564	1903.9325	1902.9252	1903.0025	-41	1	K.AHQLWLSVEALKYSMK.T
565 - 583	1930.0057	1928.9984	1928.9877	6	0	K.TSSAEMPTIPLGSAVEAIR.V
565 - 583	1946.0005	1944.9932	1944.9826	5	0	K.TSSAEMPTIPLGSAVEAIR.V Oxidation (M)
584 - 606	2534.2175	2533.2102	2533.2119	-1	0	R.VNCSDNEFTQALTAAIPPESLTR.G
607 - 615	1053.5651	1052.5578	1052.5138	42	0	R.GVYSEETLR.A
627 - 635	1090.5702	1089.5629	1089.5601	3	1	R.RVAMIDETR.N
656 - 672	2003.0452	2002.0379	2002.0411	-2	0	K.QLKPPAELYPEDINTFK.L
673 - 691	2153.0630	2152.0557	2152.0510	2	0	K.LLSYASYCIEHGDLELAAK.F
702 - 709	1015.5961	1014.5888	1014.5611	27	1	R.RVAQDWLK.E

Table W2. (*continued*)

villin 2

Score: **245** Expect: **4.5e-020**

Number of unique mass values matched: 41
Sequence Coverage: **60%**

Start - End	Observed	Mr(expt)	Mr(calc)	ppm	Miss	Sequence
9 - 27	2082.0090	2081.0017	2080.9987	1	0	R.VTTMDAELEFAIQPNTTGK.Q Oxidation (M)
28 - 35	976.5739	975.5666	975.5389	28	0	K.QLFDQVVK.T
41 - 53	1660.8175	1659.8102	1659.7933	10	0	R.EVWYFGLQYVDNK.G
65 - 72	916.5323	915.5250	915.5138	12	1	K.VSAQEVRK.E
72 - 79	989.5712	988.5639	988.5342	30	1	R.KENPVQFK.F
73 - 81	1164.5922	1163.5849	1163.6087	-20	1	K.ENPVQFKFR.A
82 - 100	2237.0789	2236.0716	2236.1263	-24	1	R.AKFYPEDVAEELIQDITQK.L
84 - 100	2038.0107	2037.0034	2036.9942	5	0	K.FYPEDVAEELIQDITQK.L
108 - 133	2809.3713	2808.3640	2808.3891	-9	0	K.DGILSDEIYCPPETAVLLGSYAVQAK.F
140 - 151	1439.7047	1438.6974	1438.6510	32	1	K.EMHKSGYLSSER.L Oxidation (M)
144 - 156	1505.7611	1504.7538	1504.7998	-31	1	K.SGYLSSERLIPQR.V
152 - 162	1364.7168	1363.7095	1363.7394	-22	1	R.LIPQRVMDQHK.L
163 - 171	1204.6127	1203.6054	1203.5632	35	1	K.LSRDQWEDR.I
172 - 180	1175.6383	1174.6310	1174.5996	27	0	R.IQVWHAEHR.G
185 - 193	1085.5432	1084.5359	1084.5110	23	0	K.DSAMLEYLK.I Oxidation (M)
194 - 209	1946.9786	1945.9713	1945.9495	11	0	K.IAQDLEMYGINYFEIK.N
194 - 209	1962.9620	1961.9547	1961.9444	5	0	K.IAQDLEMYGINYFEIK.N Oxidation (M)
238 - 246	1104.6127	1103.6054	1103.5764	26	0	K.IGFPWSEIR.N
247 - 254	965.5443	964.5370	964.4978	41	1	R.NISFNDKK.F
255 - 262	959.5816	958.5743	958.5851	-11	0	K.FVIKPIDK.K
255 - 263	1087.7021	1086.6948	1086.6801	14	1	K.FVIKPIDKK.A
263 - 273	1310.7156	1309.7083	1309.6819	20	1	K.KAPDFVFYAPR.L
264 - 273	1182.6233	1181.6160	1181.5869	25	0	K.APDFVFYAPR.L
280 - 293	1793.8982	1792.8909	1792.8422	27	0	R.ILQLCMGNHELYMR.R Oxidation (M)
280 - 293	1809.8549	1808.8476	1808.8372	6	0	R.ILQLCMGNHELYMR.R 2 Oxidation (M)
295 - 306	1488.8021	1487.7948	1487.7766	12	1	R.RKPDTIEVQQMK.A Oxidation (M)
296 - 306	1332.6926	1331.6853	1331.6755	7	0	K.KPDTIEVQQMK.A Oxidation (M)
296 - 310	1742.8824	1741.8751	1741.9145	-23	1	R.KPDTIEVQQMKAQAR.E
317 - 327	1401.7443	1400.7370	1400.7259	8	1	K.QLERQQLETEK.K
321 - 328	1003.5543	1002.5470	1002.5345	12	1	R.QQLETEKK.R
343 - 350	1063.5746	1062.5673	1062.5379	28	1	R.EKEELMLR.L Oxidation (M)
372 - 379	987.5424	986.5351	986.5032	32	0	K.ALQLEEER.R
372 - 380	1143.6357	1142.6284	1142.6043	21	1	K.ALQLEEERR.R
382 - 393	1416.6907	1415.6834	1415.6640	14	1	R.AQEEAERLEADR.M
413 - 427	1651.8317	1650.8244	1650.8100	9	0	K.SQEQLAAELAEYTAK.I
428 - 435	914.5594	913.5521	913.5232	32	0	K.IALLEEAR.R
428 - 436	1070.6385	1069.6312	1069.6243	6	1	K.IALLEEARR.R
438 - 448	1484.7191	1483.7118	1483.6691	29	1	R.KEDEVEEWQHR.A
439 - 448	1356.6317	1355.6244	1355.5742	37	0	K.EDEVEEWQHR.A
449 - 458	1116.6097	1115.6024	1115.5822	18	1	R.AKEAQDDLVK.T
530 - 542	1472.8320	1471.8247	1471.7994	17	0	R.QLLTLSNELSQAR.D
548 - 559	1493.7607	1492.7534	1492.6841	46	0	R.THNDIIHNENMR.Q
548 - 559	1509.7062	1508.6989	1508.6790	13	0	R.THNDIIHNENMR.Q Oxidation (M)
578 - 586	1138.5610	1137.5537	1137.5124	36	1	K.QRIDEFEAM.-
578 - 586	1154.5375	1153.5302	1153.5074	20	1	K.QRIDEFEAM.- Oxidation (

Table W2. (*continued*)

heat shock protein 5, GRP78, BIP

Score: **240** Expect: **1.4e-019**

Number of unique mass values matched: **36**
Sequence Coverage: **56%**

Start - End	Observed	Mr(expt)	Mr(calc)	ppm	Miss	Sequence
51 - 61	1228.6202	1227.6129	1227.6207	-6	0	R.VEIIANDQGNR.I
62 - 75	1566.7715	1565.7642	1565.7726	-5	0	R.ITPSYVAFTPEGER.L
83 - 97	1677.8042	1676.7969	1676.8006	-2	0	K.NQLTSNPENTVFDAK.R
83 - 98	1833.9252	1832.9179	1832.9017	9	1	K.NQLTSNPENTVFDAKR.L
103 - 114	1430.6766	1429.6693	1429.6838	-10	0	R.TWNDPSVQQDIK.F
124 - 139	1732.9292	1731.9219	1731.9519	-17	1	K.KTKPYIQVDIGGGQTK.T
125 - 139	1604.8522	1603.8449	1603.8570	-8	0	K.TKPYIQVDIGGGQTK.T
140 - 153	1536.7827	1535.7754	1535.7905	-10	0	K.TFAPEEISAMVLTK.M
140 - 153	1552.7710	1551.7637	1551.7854	-14	0	K.TFAPEEISAMVLTK.M Oxidation (M)
165 - 182	2016.0774	2015.0701	2015.0589	6	1	K.KVTHAVVTVPAYFNDAQR.Q
166 - 182	1887.9794	1886.9721	1886.9639	4	0	K.VTHAVVTVPAYFNDAQR.Q
183 - 198	1645.8024	1644.7951	1644.8617	-40	1	R.QATKDAGTIAGLNVMR.I
187 - 198	1217.6151	1216.6078	1216.6234	-13	0	K.DAGTIAGLNVMR.I
187 - 198	1233.6101	1232.6028	1232.6183	-13	0	K.DAGTIAGLNVMR.I Oxidation (M)
199 - 214	1659.8882	1658.8809	1658.8879	-4	0	R.IINEPTAAAIAYGLDK.R
199 - 215	1815.9974	1814.9901	1814.9890	1	1	R.IINEPTAAAIAYGLDKR.E
263 - 269	903.4670	902.4597	902.4684	-10	0	R.VMEHFIK.L
263 - 269	919.4646	918.4573	918.4633	-7	0	R.VMEHFIK.L Oxidation (M)
299 - 307	997.5024	996.4951	996.5101	-15	0	R.ALSSQHQAR.I
308 - 325	2149.0159	2148.0086	2147.9899	9	0	R.IEIESFFEGEDFSETLTR.A
326 - 337	1512.7393	1511.7320	1511.7442	-8	1	R.AKFEELNMDLFR.S
326 - 337	1528.7340	1527.7267	1527.7391	-8	1	R.AKFEELNMDLFR.S Oxidation (M)
328 - 337	1313.6123	1312.6050	1312.6122	-5	0	K.FEELNMDLFR.S
328 - 337	1329.6118	1328.6045	1328.6071	-2	0	K.FEELNMDLFR.S Oxidation (M)
354 - 368	1588.8383	1587.8310	1587.8468	-10	1	K.KSDIDEIVLVGGSTR.I
355 - 368	1460.7462	1459.7389	1459.7518	-9	0	K.SDIDEIVLVGGSTR.I
378 - 387	1210.5690	1209.5617	1209.5778	-13	1	K.EFFNGKEPSR.G
448 - 465	1965.0668	1964.0595	1964.0215	19	1	K.KSQIFSTASDNQPTVTIK.V
449 - 465	1836.9268	1835.9195	1835.9265	-4	0	K.SQIFSTASDNQPTVTIK.V
466 - 475	1191.6201	1190.6128	1190.6295	-14	0	K.VYEGERPLTK.D
476 - 493	1934.0173	1933.0100	1933.0058	2	0	K.DNHLLGTFDLTGIPPAPR.G
494 - 511	1999.0449	1998.0376	1998.0786	-21	0	R.GVPQIEVTFEIDVNGIIR.V
534 - 541	986.5020	985.4947	985.5080	-13	0	R.LTPEEIER.M
542 - 554	1525.6866	1524.6793	1524.6766	2	1	R.MVNDAEKFAEEDK.K
564 - 574	1316.6240	1315.6167	1315.6295	-10	0	R.NELESYAYSLK.N
564 - 580	1972.0381	1971.0308	1970.9585	37	1	R.NELESYAYSLKNQIGDK.E
593 - 602	1193.6044	1192.5971	1192.5645	27	1	K.ETMEKAVEEK.I
603 - 618	1974.9236	1973.9163	1973.9007	8	0	K.IEWLESHQDADIEDFK.A
603 - 620	2174.0360	2173.0287	2173.0327	-2	1	K.IEWLESHQDADIEDFKAK.K
623 - 634	1397.7736	1396.7663	1396.7813	-11	0	K.ELEEIVQPIISK.L
635 - 655	2177.9883	2176.9810	2176.9648	7	1	K.LYGSGGPPPTGEEDTSEKDEL.-

Table W2. (*continued*)

heat shock protein 1

Score: **129** Expect: **1.8e-008**

Number of unique mass values matched: **29**
Sequence Coverage: **51%**

Start - End	Observed	Mr(expt)	Mr(calc)	ppm	Miss	Sequence
42 - 58	1949.9768	1948.9695	1949.0105	-21	1	K.EIFLRELISNSSDALDK.I
47 - 60	1560.8112	1559.8039	1559.8155	-7	1	R.ELISNSSDALDKIR.Y
59 - 69	1308.6798	1307.6725	1307.6721	0	1	K.IRYESLTDPSK.L
75 - 84	1163.6835	1162.6762	1162.6710	5	0	K.ELHINLIPSK.Q
75 - 87	1562.8463	1561.8390	1561.8576	-12	1	K.ELHINLIPSKQDR.T
88 - 100	1349.6902	1348.6829	1348.7272	-33	0	R.TLTIVDTGIGMTK.A
88 - 100	1365.7347	1364.7274	1364.7221	4	0	R.TLTIVDTGIGMTK.A Oxidation (M)
101 - 112	1242.7079	1241.7006	1241.6979	2	0	K.ADLINNLGTIAK.S
154 - 173	2255.9658	2254.9585	2254.9516	3	0	K.HNDDEQYAWESSAGGSFTVR.T
174 - 185	1249.6283	1248.6210	1248.5769	35	1	R.TDTGEPMGRGTK.V
186 - 201	2015.0460	2014.0387	2014.0371	1	1	K.VILHLKEDQTEYLEER.R
192 - 201	1311.6171	1310.6098	1310.5626	36	0	K.EDQTEYLEER.R
210 - 224	1778.9131	1777.9058	1777.9403	-19	0	K.HSQFIGYPITLFVEK.E
285 - 293	1151.5782	1150.5709	1150.5506	18	0	K.YIDQEELNK.T
294 - 300	901.5515	900.5442	900.5181	29	0	K.TKPIWTR.N
301 - 315	1833.7950	1832.7877	1832.7741	7	0	R.NPDDITNEEYGEFYK.S
316 - 328	1541.7775	1540.7702	1540.7522	12	0	K.SLTNDWEEHLAVK.H
329 - 339	1348.6805	1347.6732	1347.6572	12	0	K.HFSVEGQLEFR.A
347 - 356	1264.6609	1263.6536	1263.6360	14	1	R.RAPFDLFENR.K
348 - 356	1108.5677	1107.5604	1107.5349	23	0	R.APFDLFENR.K
348 - 357	1236.6509	1235.6436	1235.6299	11	1	R.APFDLFENRK.K
369 - 387	2415.1660	2414.1587	2414.1650	-3	0	R.VFIMDNCEELIPEYLNFIR.G
388 - 401	1513.8016	1512.7943	1512.7784	11	0	R.GVVDSEDLPLNISR.E
388 - 408	2374.1216	2373.1143	2373.1846	-30	1	R.GVVDSEDLPLNISREMLQQSK.I Oxidation (M)
448 - 457	1168.6049	1167.5976	1167.5632	29	0	K.LGIHEDSQNR.K
448 - 458	1296.6459	1295.6386	1295.6582	-15	1	K.LGIHEDSQNRK.K
466 - 479	1550.7599	1549.7526	1549.6970	36	0	R.YYTSASGDEMVSLK.D
487 - 500	1707.8091	1706.8018	1706.8628	-36	1	K.ENQKHIYFITGETK.D
491 - 500	1208.6445	1207.6372	1207.6237	11	0	K.HIYFITGETK.D
501 - 511	1235.6523	1234.6450	1234.5942	41	0	K.DQVANSAFVER.L

Table W2. (*continued*)

heterogeneous nuclear ribonucleoprotein L

Score: **174** Expect: **5.7e-013**

Number of unique mass values matched: **22**
Sequence Coverage: **47%**

Start - End	Observed	Mr(expt)	Mr(calc)	ppm	Miss	Sequence
29 - 46	1475.7546	1474.7473	1474.7133	23	1	R.AGAMVKMAAAGGGGGGGR.Y
29 - 46	1491.7107	1490.7034	1490.7082	-3	1	R.AGAMVKMAAAGGGGGGGR.Y Oxidation (M)
47 - 56	1029.4589	1028.4516	1028.4312	20	0	R.YYGGGNEGGR.A
63 - 94	2840.1410	2839.1337	2839.1415	-3	0	K.TENAGDQHGGGGGGGSGAAGGGGGENYDDPHK.T
95 - 104	1076.6338	1075.6265	1075.6138	12	0	K.TPASPVVHIR.G
176 - 186	1204.5929	1203.5856	1203.5480	31	0	K.ISRPGDSDDSR.S
226 - 243	1993.9883	1992.9810	1992.9687	6	1	R.KNGVQAMVEFDSVQSAQR.A
226 - 243	2009.9849	2008.9776	2008.9636	7	1	R.KNGVQAMVEFDSVQSAQR.A Oxidation (M)
227 - 243	1865.9003	1864.8930	1864.8738	10	0	K.NGVQAMVEFDSVQSAQR.A
227 - 243	1881.8894	1880.8821	1880.8687	7	0	K.NGVQAMVEFDSVQSAQR.A Oxidation (M)
246 - 261	1729.8187	1728.8114	1728.7811	18	0	K.ASLNGADIYSGCCTLK.I
262 - 269	977.5530	976.5457	976.5341	12	0	K.IEYAKPTR.L
275 - 300	2890.2610	2889.2537	2889.2550	-0	1	K.NDQDTWDYTNPNLSGQGDPGSNPNKR.Q
342 - 350	907.4661	906.4588	906.4494	10	0	R.MGPPVGGHR.R
342 - 350	923.4672	922.4599	922.4443	17	0	R.MGPPVGGHR.R Oxidation (M)
342 - 351	1063.5692	1062.5619	1062.5505	11	1	R.MGPPVGGHRR.G
342 - 351	1079.5763	1078.5690	1078.5454	22	1	R.MGPPVGGHRR.G Oxidation (M)
396 - 408	1588.7927	1587.7854	1587.7756	6	0	R.VFNVFCLYGNVEK.V
396 - 410	1815.9719	1814.9646	1814.9389	14	1	R.VFNVFCLYGNVEKVK.F
414 - 431	1867.8966	1866.8893	1866.8604	15	0	K.SKPGAAMVEMADGYAVDR.A
414 - 431	1883.8937	1882.8864	1882.8553	17	0	K.SKPGAAMVEMADGYAVDR.A Oxidation (M)
414 - 431	1899.8689	1898.8616	1898.8502	6	0	K.SKPGAAMVEMADGYAVDR.A 2 Oxidation (M)
432 - 445	1634.8174	1633.8101	1633.8035	4	0	R.AITHLNNNFMFGQK.M
432 - 445	1650.8053	1649.7980	1649.7984	-0	0	R.AITHLNNNFMFGQK.M Oxidation (M)
453 - 472	2187.9920	2186.9847	2186.9612	11	0	K.QPAIMPGQSYGLEDGSCSYK.D
453 - 472	2203.9854	2202.9781	2202.9562	10	0	K.QPAIMPGQSYGLEDGSCSYK.D Oxidation (M)
453 - 478	2909.2666	2908.2593	2908.2644	-2	1	K.QPAIMPGQSYGLEDGSCSYKDFSESR.N
539 - 549	1208.5940	1207.5867	1207.5721	12	0	R.SSSGLLEWDSK.S
550 - 565	1866.8724	1865.8651	1865.8982	-18	0	K.SDALETLGFLNHYQMK.N
550 - 565	1882.8845	1881.8772	1881.8931	-8	0	K.SDALETLGFLNHYQMK.N Oxidation (M)
566 - 576	1263.6481	1262.6408	1262.6295	9	0	K.NPNGPYPYTLK.L
577 - 586	1121.5149	1120.5076	1120.4971	9	0	K.LCFSTAQHAS.-

Table W2. (*continued*)

heterogeneous nuclear ribonucleoprotein K

Score: **119** Expect: **1.8e-007**

Number of unique mass values matched: **18**
Sequence Coverage: **41%**

Start - End	Observed	Mr(expt)	Mr(calc)	ppm	Miss	Sequence
22 - 34	1579.7118	1578.7045	1578.6984	4	0	K.RPAEDMEEEQAFK.R
22 - 34	1595.7205	1594.7132	1594.6933	12	0	K.RPAEDMEEEQAFK.R Oxidation (M)
22 - 35	1735.8105	1734.8032	1734.7995	2	1	K.RPAEDMEEEQAFKR.S
22 - 35	1751.8088	1750.8015	1750.7944	4	1	K.RPAEDMEEEQAFKR.S Oxidation (M)
36 - 46	1349.6874	1348.6801	1348.6405	29	1	R.SRNTDEMVELR.I
38 - 46	1106.5227	1105.5154	1105.5074	7	0	R.NTDEMVELR.I
70 - 86	1780.8070	1779.7997	1779.7911	5	0	R.TDYNASVSVPDSSGPER.I
87 - 102	1714.9431	1713.9358	1713.9764	-24	0	R.ILSISADIETIGEILK.K
87 - 103	1843.0535	1842.0462	1842.0713	-14	1	R.ILSISADIETIGEILKK.I
140 - 148	1098.4559	1097.4486	1097.4448	4	0	K.GSDFDCELR.L
149 - 163	1518.9264	1517.9191	1517.9293	-7	0	R.LLIHQSLAGGIIGVK.G
180 - 191	1549.6561	1548.6488	1548.6450	2	0	K.LFQECCPHSTDR.V
192 - 201	1053.6368	1052.6295	1052.6342	-4	0	R.VVLIGGKPDR.V
208 - 219	1340.7977	1339.7904	1339.7962	-4	0	K.IILDLISESPIK.G
306 - 316	1194.6909	1193.6836	1193.6921	-7	0	R.NLPLPPPPPPR.G
317 - 325	997.4449	996.4376	996.4335	4	0	R.GGDLMAYDR.R
317 - 326	1153.5441	1152.5368	1152.5346	2	1	R.GGDLMAYDRR.G
317 - 326	1169.5442	1168.5369	1168.5295	6	1	R.GGDLMAYDRR.G Oxidation (M)
378 - 396	1917.0377	1916.0304	1916.0255	3	0	R.GSYGDLGGPIITTQVTIPK.D
423 - 433	1259.6279	1258.6206	1258.5677	42	0	K.IDEPLEGSEDR.I
434 - 456	2589.3845	2588.3772	2588.3810	-1	0	R.IITITGTQDQIQNAQYLLQNSVK.Q

Table W2. (*continued*)

vimentin

Score: **225** Expect: **4.5e-018**

Number of unique mass values matched: **31**
Sequence Coverage: **59%**

Start - End	Observed	Mr(expt)	Mr(calc)	ppm	Miss	Sequence
59 - 77	2126.0708	2125.0635	2125.0579	3	0	R.LLQDSVDFSLADAINTEFK.N
81 - 93	1587.8036	1586.7963	1586.7900	4	1	R.TNEKVELQELNDR.F
85 - 93	1115.5687	1114.5614	1114.5618	-0	0	K.VELQELNDR.F
110 - 119	1169.7110	1168.7037	1168.7067	-3	0	K.ILLAELEQLK.G
110 - 123	1539.9098	1538.9025	1538.9032	-0	1	K.ILLAELEQLKGQGK.S
124 - 135	1497.7247	1496.7174	1496.6929	16	1	K.SRLGDLYEEEMR.E
126 - 135	1254.5704	1253.5631	1253.5598	3	0	R.LGDLYEEEMR.E
126 - 135	1270.5632	1269.5559	1269.5547	1	0	R.LGDLYEEEMR.E Oxidation (M)
151 - 164	1688.8242	1687.8169	1687.8199	-2	1	R.VEVERDNLAEDIMR.L
151 - 164	1704.8322	1703.8249	1703.8148	6	1	R.VEVERDNLAEDIMR.L Oxidation (M)
156 - 164	1076.5090	1075.5017	1075.4968	5	0	R.DNLAEDIMR.L
167 - 176	1303.6754	1302.6681	1302.6601	6	1	R.EKLQEEMLQR.E
167 - 176	1319.6547	1318.6474	1318.6551	-6	1	R.EKLQEEMLQR.E Oxidation (M)
169 - 176	1046.5367	1045.5294	1045.5226	7	0	K.LQEEMLQR.E
169 - 187	2324.1113	2323.1040	2323.1114	-3	1	K.LQEEMLQREEAESTLQSFR.Q
177 - 187	1296.6482	1295.6409	1295.5993	32	0	R.EEAESTLQSFR.Q
204 - 215	1405.7172	1404.7099	1404.7500	-29	0	K.VESLQEEIAFLK.K
204 - 216	1533.8573	1532.8500	1532.8450	3	1	K.VESLQEEIAFLKK.L
263 - 272	1309.6221	1308.6148	1308.5986	12	0	K.NLQEAEEWYK.S
273 - 284	1308.6484	1307.6411	1307.6469	-4	1	K.SKFADLSEAANR.N
275 - 284	1093.5385	1092.5312	1092.5200	10	0	K.FADLSEAANR.N
294 - 301	1081.5227	1080.5154	1080.4948	19	1	K.QESNEYRR.Q
302 - 314	1490.7515	1489.7442	1489.7446	-0	0	R.QVQSLTCEVDALK.G
302 - 322	2377.1685	2376.1612	2376.1591	1	1	R.QVQSLTCEVDALKGTNESLER.Q
326 - 344	2200.9910	2199.9837	2199.9742	4	0	R.EMEENFALEAANYQDTIGR.L
326 - 344	2216.9970	2215.9897	2215.9691	9	0	R.EMEENFALEAANYQDTIGR.L Oxidation (M)
345 - 358	1734.8265	1733.8192	1733.8076	7	1	R.LQDEIQNMKEEMAR.H
345 - 358	1750.8184	1749.8111	1749.8025	5	1	R.LQDEIQNMKEEMAR.H Oxidation (M)
345 - 358	1766.8461	1765.8388	1765.7974	23	1	R.LQDEIQNMKEEMAR.H 2 Oxidation (M)
362 - 370	1121.5856	1120.5783	1120.5764	2	0	R.EYQDLLNVK.M
371 - 381	1295.6661	1294.6588	1294.6591	-0	0	K.MALDIEIATYR.K
371 - 381	1311.6470	1310.6397	1310.6540	-11	0	K.MALDIEIATYR.K Oxidation (M)
371 - 382	1423.7529	1422.7456	1422.7540	-6	1	K.MALDIEIATYRK.L
382 - 390	1060.5632	1059.5559	1059.5560	-0	1	R.KLLEGEESR.I
391 - 404	1557.9036	1556.8963	1556.8926	2	0	R.ISLPLPTFSSLNLR.E
405 - 419	1682.8700	1681.8627	1681.8523	6	0	R.ETNLESLPLVDTHSK.R
405 - 420	1838.9209	1837.9136	1837.9534	-22	1	R.ETNLESLPLVDTHSKR.T
431 - 446	1836.8154	1835.8081	1835.7922	9	0	R.DGQVINETSQHHDDLE.-

Table W2. (*continued*)

Lap3

Score: **151** Expect: **1.1e-010**

Number of unique mass values matched: **27**
Sequence Coverage: **56%**

Start - End	Observed	Mr(expt)	Mr(calc)	ppm	Miss	Sequence
1 - 11	1215.6342	1214.6269	1214.6845	-47	0	-.MYLLPLPAAAR.V
1 - 11	1231.6321	1230.6248	1230.6794	-44	0	-.MYLLPLPAAAR.V Oxidation (M)
35 - 43	933.5963	932.5890	932.5695	21	0	K.GLVLGIYAK.D
67 - 79	1467.8285	1466.8212	1466.8279	-5	1	K.LREMLNISGPPLK.A
67 - 79	1483.8193	1482.8120	1482.8228	-7	1	K.LREMLNISGPPLK.A Oxidation (M)
69 - 79	1198.6508	1197.6435	1197.6427	1	0	R.EMLNISGPPLK.A
69 - 79	1214.6564	1213.6491	1213.6376	9	0	R.EMLNISGPPLK.A Oxidation (M)
85 - 103	2063.0933	2062.0860	2062.0888	-1	0	R.TFYGLHQDFPSVVVVGLGK.R
105 - 118	1571.7098	1570.7025	1570.6648	24	0	R.SAGVDDQENWHEGK.E
105 - 122	2083.9670	2082.9597	2082.9355	12	1	R.SAGVDDQENWHEGKENIR.A
177 - 188	1341.6648	1340.6575	1340.6361	16	0	K.LHGSGDLEAWEK.G
189 - 200	1232.6888	1231.6815	1231.6673	12	0	K.GVLFASGQNLAR.H
201 - 214	1613.7680	1612.7607	1612.7337	17	0	R.HLMESPANEMTPTR.F
201 - 214	1629.7711	1628.7638	1628.7287	22	0	R.HLMESPANEMTPTR.F Oxidation (M)
201 - 214	1645.7744	1644.7671	1644.7236	26	0	R.HLMESPANEMTPTR.F 2 Oxidation (M)
238 - 253	1840.9200	1839.9127	1839.8713	23	0	K.SWIEEQEMGSFLSVAK.G
238 - 253	1856.9084	1855.9011	1855.8662	19	0	K.SWIEEQEMGSFLSVAK.G Oxidation (M)
283 - 294	1194.6176	1193.6103	1193.6292	-16	0	K.GITFDSGGISIK.A
295 - 303	1008.4924	1007.4851	1007.4528	32	0	K.ASANMDLMR.A
304 - 321	1693.8310	1692.8237	1692.8175	4	0	R.ADMGGAATICSAIVSAAK.L
304 - 321	1709.8375	1708.8302	1708.8124	10	0	R.ADMGGAATICSAIVSAAK.L Oxidation (M)
322 - 342	2264.1758	2263.1685	2263.2068	-17	0	K.LNLPINIIGLAPLCENMPSGK.A
322 - 342	2280.1638	2279.1565	2279.2017	-20	0	K.LNLPINIIGLAPLCENMPSGK.A Oxidation (M)
343 - 351	955.5510	954.5437	954.5247	20	0	K.ANKPGDVVR.A
357 - 368	1318.6875	1317.6802	1317.6161	49	0	K.TIQVDNTDAEGR.L
369 - 384	1846.9454	1845.9381	1845.9447	-4	0	R.LILADALCYAHTFNPK.V
418 - 428	1223.6074	1222.6001	1222.5830	14	0	K.LFEASVETGDR.V
418 - 431	1664.9064	1663.8991	1663.8318	40	1	K.LFEASVETGDRVWR.M
432 - 440	1193.5958	1192.5885	1192.5699	16	0	R.MPLFEHYTR.Q
432 - 440	1209.5900	1208.5827	1208.5648	15	0	R.MPLFEHYTR.Q Oxidation (M)
441 - 455	1686.8605	1685.8532	1685.8407	7	0	R.QVIDCQLADVNNLGK.Y
458 - 469	1195.6106	1194.6033	1194.5815	18	0	R.SAGACTAAAFLR.E
490 - 496	905.5000	904.4927	904.4654	30	0	K.DEIPYLR.K
490 - 497	1033.5830	1032.5757	1032.5604	15	1	K.DEIPYLRK.G
497 - 505	989.5490	988.5417	988.5236	18	1	R.KGMSGRPTR.T
506 - 513	1004.6306	1003.6233	1003.6066	17	0	R.TLIEFLLR.F

lectin, galactose binding, soluble 3

Score: **122** Expect: **9.1e-008**

Number of unique mass values matched: **9**
Sequence Coverage: **80%**

Start - End	Observed	Mr(expt)	Mr(calc)	ppm	Miss	Sequence
4 - 18	1658.9167	1657.9094	1657.9007	5	0	R.MLITIMGTVKPNANR.I
4 - 18	1674.9080	1673.9007	1673.8957	3	0	R.MLITIMGTVKPNANR.I Oxidation (M)
4 - 18	1690.8987	1689.8914	1689.8906	1	0	R.MLITIMGTVKPNANR.I 2 Oxidation (M)
25 - 36	1429.7160	1428.7087	1428.7011	5	1	R.RGNDVAFHFNPR.F
26 - 36	1273.6036	1272.5963	1272.6000	-3	0	R.GNDVAFHFNPR.F
37 - 43	949.4670	948.4597	948.4525	8	1	R.FNENNRR.V
43 - 50	989.5470	988.5397	988.5488	-9	1	R.RVIVCNTK.Q
61 - 73	1469.7491	1468.7418	1468.7351	5	0	R.QSAFPFESGKPFK.I
74 - 84	1298.7118	1297.7045	1297.7030	1	0	K.IQVLVEADHFK.V
85 - 98	1649.8639	1648.8566	1648.8434	8	0	K.VAVNDAHLLQYNHR.M
104 - 124	2171.1120	2170.1047	2170.0940	5	0	R.EISQLGISGDITLTSANHAMI.-
104 - 124	2187.0984	2186.0911	2186.0889	1	0	R.EISQLGISGDITLTSANHAMI.- Oxidation (M)

Table W2. (*continued*)

aldolase 1, A isoform

Unique Queries matched: 7

Observed	Mr(expt)	Mr(calc)	Delta	Miss	Score	Expect	Rank	Peptide
464.1914	926.3682	926.4168	-0.0485	0	42	0.0092	1	R.CQYVTEK.V
476.2231	950.4316	950.4709	-0.0392	0	29	0.35	1	K.AAQEEYIK.R
522.7621	1043.5097	1043.5611	-0.0514	0	68	4e-005	1	R.QLLLTADDR.V
566.7627	1131.5107	1131.5706	-0.0599	0	93	1.3e-007	1	R.ALANSLACQGK.Y
666.8208	1331.6270	1331.6932	-0.0662	0	88	3.8e-007	1	K.GILAADESTGSIAK.R
745.8178	1489.6211	1489.7008	-0.0797	0	77	2.3e-006	1	R.LQSIGTENTEENR.R
549.5741	1645.7006	1645.8019	-0.1013	1	23	0.59	1	R.LQSIGTENTEENRR.F

procollagen-lysine, 2-oxoglutarate 5-dioxygenase 3

Unique Queries matched: 4

Observed	Mr(expt)	Mr(calc)	Delta	Miss	Score	Expect	Rank	Peptide
530.2870	1058.5595	1058.5509	0.0086	0	68	3.9e-005	1	R.TLGLGQEWR.G
535.2190	1068.4234	1068.4295	-0.0061	0	46	0.004	1	K.GVDYEGGGCR.F
619.3055	1236.5964	1236.5986	-0.0022	0	38	0.032	1	R.SEDYVELVQR.K
699.8605	1397.7064	1397.7150	-0.0087	0	108	3.2e-009	1	K.LVGPEEALSAGEAR.D

Table W2. (*continued*)

vinculin

Unique Queries matched: 16

Observed	Mr(expt)	Mr(calc)	Delta	Miss	Score	Expect	Rank	Peptide
500.8037	999.5928	999.5964	-0.0036	0	72	1.6e-005	1	R.IPTISTQLK.I
511.2799	1020.5452	1020.5273	0.0178	1	50	0.0029	1	R.KLEAMTNSK.Q
537.2753	1072.5361	1072.5335	0.0025	0	55	0.00088	1	R.GQGASPVAMQK.A
545.3164	1088.6182	1088.6077	0.0105	0	85	8.6e-007	1	R.SLGEIAALTSK.L
559.8107	1117.6069	1117.5979	0.0090	0	56	0.00055	1	K.STVEGIQASVK.T
566.7986	1131.5826	1131.5706	0.0120	0	60	0.0003	1	R.TNLLQVCER.I
587.3320	1172.6494	1172.6401	0.0093	0	93	1.3e-007	1	R.ALASQLQDSLK.D
588.3175	1174.6205	1174.6016	0.0189	0	53	0.0014	1	K.MSAEINEIIR.V
592.8393	1183.6641	1183.6561	0.0080	0	47	0.0048	1	R.ELTPQVISAAR.I
618.3304	1234.6463	1234.6414	0.0050	0	60	0.00023	1	R.VMLVNSMNTVK.E
635.3468	1268.6791	1268.6725	0.0067	0	69	2.5e-005	1	K.AVAGNISDPGLQK.S
646.8314	1291.6482	1291.6330	0.0152	0	71	1.9e-005	1	K.MTGLVDEAIDTK.S
657.8700	1313.7255	1313.7303	-0.0048	0	97	4e-008	1	K.QVATALQNLQTK.T
702.8710	1403.7275	1403.7144	0.0131	0	56	0.00046	1	K.ETVQTTEDQILK.R
729.4068	1456.7990	1456.7886	0.0104	0	100	1.8e-008	1	K.AQQVSQGLDVLTAK.V
749.3532	1496.6918	1496.6855	0.0063	0	93	9.2e-008	1	R.DPNASPGDAGEQAIR.Q